**RESEARCH ARTICLE**

# A weather system perspective on winter–spring rainfall variability in southeastern Australia during El Niño

Seraphine Hauser[1] | Christian M. Grams[1] | Michael J. Reeder[2] |
Shayne McGregor[2] | Andreas H. Fink[1] | Julian F. Quinting[1]

[1]Institute of Meteorology and Climate Research (IMK-TRO), Department Troposphere Research, Karlsruhe Institute of Technology (KIT), Karlsruhe, Germany

[2]School of Earth, Atmosphere and Environment, and ARC Centre of Excellence for Climate Extremes, Monash University, Clayton, Victoria, Australia

**Correspondence**
S. Hauser, Institute of Meteorology and Climate Research (IMK-TRO), Department of Troposphere Research, KIT, PO 3640, Karlsruhe 76021, Germany.
Email: seraphine.hauser@kit.edu

**Funding information**
Australian Research Council Centre of Excellence for Climate Extremes, Grant/Award Number: CE170100023; Deutsche Forschungsgemeinschaft, Grant/Award Number: SFB/TRR 165; Helmholtz Association, Grant/Award Number: VH-NG-1243

**Abstract**

The El Niño phase of the El Niño Southern Oscillation (ENSO) is typically associated with below-average cool-season rainfall in southeastern Australia (SEA). However, there is also large case-to-case variability on monthly time-scales. Despite recent progress in understanding the links between remote climate drivers and this variability, the underlying dynamical processes are not fully understood. This reanalysis-based study aims to advance the dynamical understanding by quantifying the contribution of midlatitude weather systems to monthly precipitation anomalies over SEA during the austral winter–spring season. A k-means clustering reveals four rainfall anomaly patterns with above-average rainfall (Cluster 1), below-average rainfall (Cluster 2), above-average rainfall along the East Coast (Cluster 3) and along the South Coast (Cluster 4). Cluster 2 occurs most frequently during El Niño, which highlights the general suppression of SEA rainfall during these events. However, the remaining three clusters with local above-average rainfall are found in ∼52% of all El Niño months. Changes of weather system frequency determine the respective rainfall anomaly pattern. Results indicate significantly more cut-off lows and warm conveyor belts (WCBs) over SEA in El Niño Cluster 1 and significantly fewer in El Niño Cluster 2. In El Niño Cluster 3, enhanced blocking south of Australia favours cut-off lows leading to increased rainfall along the East Coast. Positive rainfall anomalies along the South Coast in El Niño Cluster 4 are associated with frontal rainfall due to an equatorward shift of the midlatitude storm track. Most of the rainfall is produced by WCBs and cut-off lows but the contributions strongly vary between the clusters. In all clusters, rainfall anomalies result from changes in rainfall frequency more than in rainfall intensity. Backward trajectories of WCB and cut-off low rainfall highlight the importance of moist air masses from the Coral Sea and the northwest coast of Australia during wet months.

**KEYWORDS**

backward trajectories, clustering, El Niño, rainfall decomposition, rainfall origin, rainfall variability, southeastern Australia, synoptic weather systems

# 1 | INTRODUCTION

The rainfall variability in southeastern Australia (SEA) is notable for its magnitude compared to other places in the world that are located in similar climate zones (Nicholls *et al.*, 1997). Hence, potential drivers of this variability have been the subject of many studies (e.g., Nicholls *et al.*, 1997; Power *et al.*, 1999; Murphy and Timbal, 2008; Risbey *et al.*, 2009b, Risbey *et al.*, 2013, King *et al.*, 2014). Drivers of rainfall variability in Australia can be split into two categories based on their temporal and spatial extent: lower-frequency processes including both large-scale atmospheric and oceanic phenomena, and higher-frequency processes on the synoptic scale referred to as synoptic systems (Risbey *et al.*, 2009b). Of course, this separation is not clear-cut, as large-scale drivers additionally affect drivers on the smaller scales and *viceversa* (King *et al.*, 2014).

The lower-frequency remote drivers of intraseasonal-to-interannual rainfall variability are the El Niño–Southern Oscillation (ENSO), the Indian Ocean Dipole (IOD) and the Southern Annular Mode (SAM) (e.g., McBride and Nicholls, 1983; Nicholls *et al.*, 1996; Murphy and Timbal, 2008; Risbey *et al.*, 2009b; Cowan *et al.*, 2013), although the relevance of SAM to Southern Hemisphere midlatitude variability has been questioned recently (Spensberger *et al.*, 2020). ENSO explains most of the interannual rainfall variability in Australia and its influence on rainfall is consistent through the seasons (Risbey *et al.*, 2009b). Winter–spring rainfall (JJASON) is usually reduced during El Niño and enhanced during La Niña in the eastern and extreme southern parts of Australia (e.g., McBride and Nicholls, 1983; Allan *et al.*, 1996; Nicholls *et al.*, 1996; Murphy and Timbal, 2008; Risbey *et al.*, 2009a, 2009b; Chung and Power, 2017). The preferred occurrence of positive SAM during La Niña and of negative SAM during El Niño points to a significant relationship between SAM and ENSO (Fogt *et al.*, 2011). However, the strong El Niño event of 2015/2016 that co-occurred with a positive SAM phase has questioned the relationship and suggests a multidecadal variation of the connection (Vera and Osman, 2018). In most of the regions in Australia, one or two large-scale climate modes dominate rainfall variability, however SEA is an exception due to the complex combination of local topography and additional large-scale remote drivers (Risbey *et al.*, 2009b; Ashcroft *et al.*, 2016). For example, rainfall variability in spring and autumn is influenced by ENSO, IOD, SAM and atmospheric blocking (Risbey *et al.*, 2009b). In addition to the large-scale climate modes, synoptic weather systems are the high-frequency drivers of submonthly rainfall variability. SEA receives the majority of its annual rainfall in the winter half, which is important for the growing season from April to November (Pook *et al.*, 2006; Murphy and Timbal, 2008). Extratropical cyclones and the passage of cold fronts influence rainfall along the southeastern coastal regions and cut-off lows and tropical–extratropical interactions manifested as northwest cloudbands contribute to rainfall more inland (Tapp and Barrell, 1984; Wright, 1997; Murphy and Timbal, 2008).

The relationship of rainfall in SEA with El Niño is weaker than the relationship with La Niña (Power *et al.*, 2006; Murphy and Timbal, 2008; King *et al.*, 2014; Chung and Power, 2017). The magnitude of the sea surface temperature (SST) anomalies associated with the El Niño events of 1982 and 1997 were similar but resulted in different rainfall responses in Australia. In 1982, El Niño conditions were associated with a devastating drought in Australia. The El Niño of 1997 exceeded the magnitude of the 1982 event, yet was associated with only slightly below-average rainfall over east Australia (Brown *et al.*, 2009; Taschetto and England, 2009; van Rensch *et al.*, 2019). The different responses point to the nonlinear relationship between El Niño strength and the impact on SEA rainfall, and reveals that the strength of El Niño alone might be a poor predictor for rainfall deficiency (Power *et al.*, 2006). Regarding El Niño in particular, there is a lack of knowledge about the processes that drive interannual rainfall variability in east Australia (Brown *et al.*, 2009; van Rensch *et al.*, 2019). For these reasons, the varying processes that link El Niño and rainfall in SEA require further examination (van Rensch *et al.*, 2019).

Previous studies on rainfall variability in SEA document statistical relationships between large-scale climate modes and rainfall in this region (e.g., Taschetto and England, 2009; Risbey *et al.*, 2009b; Ashcroft *et al.*, 2016). However, a weather system approach has recently contributed to considerable progress in understanding the North Atlantic Oscillation and precipitation response to ENSO over the North Atlantic, leading to the impression that weather systems shape a significant fraction of the ENSO teleconnection (Li and Lau, 2012; Drouard *et al.*, 2015; Schemm *et al.*, 2018). We therefore take a different approach in this study which aims to advance a meteorological understanding of processes during El Niño. Instead of focusing on entire El Niño events or seasons, we investigate the monthly rainfall anomaly patterns in SEA. Clustering these anomalies allows a detailed analysis of the processes involved. We investigate the effect of weather systems on rainfall variability during El Niño by addressing the following questions:

- What are the monthly rainfall anomaly patterns during the winter–spring season in SEA and how does the

occurrence of these patterns change during El Niño events?

- How do weather system frequencies over Australia change during El Niño?
- How are weather systems related to observed rainfall anomaly patterns and which weather systems produce rainfall in SEA during El Niño?
- Where is the origin of air masses during rainfall?

The paper is structured in the following manner. In the next section, we describe the datasets and methods. In Section 3, we first introduce the rainfall anomaly clusters over SEA, followed by a weather system perspective on rainfall variability and a broader view on the origin of rainfall during El Niño. Section 4 discusses the results of this study with previous findings. In Section 5, we conclude and give a brief summary with further directions for future work.

## 2 | DATA AND METHODOLOGY

### 2.1 | Daily rainfall data

Daily gridded Australian Water Availability Project (AWAP) rainfall data are taken from the Australian Data Archive for Meteorology at a spatial resolution of $0.05° \times 0.05°$ (Jones *et al.*, 2009). Total daily rainfall is accumulated in the 24-hr period starting at 0900 am (local time) the day before. The monthly reference climatology used to compute monthly anomalies is 1961–1990, which is the same as that used by the Bureau of Meteorology.

### 2.2 | ERA-Interim reanalysis and objectively identified weather systems

An essential data source for this study is the ERA-Interim reanalysis produced by the European Centre for Medium-Range Weather Forecasts (ECMWF; Berrisford *et al.*, 2009; Dee *et al.*, 2011). For the considered time period 1979–2015, 6-hourly ERA-Interim reanalyses are used and remapped to a regular latitude–longitude grid with 1° horizontal grid spacing.

An ERA-Interim-based dataset of objectively identified flow features allows the analysis of the occurrence frequency of midlatitude weather systems (Sprenger *et al.*, 2017). The collection provides six-hourly two-dimensional binary fields of the different flow feature masks. Monthly mean data are available and accessible via the web portal (http://eraiclim.ethz.ch; accessed 25 April 2020). The dataset for this study includes cyclones

(Pasquier *et al.*, 2019), cut-off lows (at 315 and 320 K; Wernli and Schwierz, 2006; Wernli and Sprenger, 2007), atmospheric blocking (with the use of the 0.7 PVU anomaly that persists for at least 5 days; Schwierz *et al.*, 2004), regions of anomalous moisture transport excluding the tropical belt (20°S–20°N; Pasquier *et al.*, 2019) and warm conveyor belts (WCBs; Madonna *et al.*, 2014). WCBs are the main precipitating and ascending airstreams associated with extratropical cyclones (Browning, 1990). Here, WCBs are identified by trajectories which need to ascend at least 600 hPa in 48 hr. We consider the WCB at the beginning (WCB inflow, pressure level of trajectories > 800 hPa), at its main ascending part (WCB ascent, pressure level of trajectories between 800 and 400 hPa) and at the end of the their ascent phase (WCB outflow, pressure level of trajectories < 400 hPa) separately. Further extratropical weather features which are associated with precipitation are cold fronts (Catto *et al.*, 2012a, Catto *et al.*, 2015) which are also included as part of the dataset of Sprenger *et al.* (2017). However, cold fronts in Australia do not necessarily bring rainfall in winter but WCB rainfall is relatively common in the spring season (Reeder and Smith, 1998). For this reason, we choose to focus our analysis on WCBs instead of surface cold fronts. An example to introduce the flow feature dataset to the reader is given in Figure 1b. Anomalies of occurrence frequencies are calculated relative to the monthly climatology for the period 1979–2015. In the following, we use the term "weather systems" for our dataset of flow features.

### 2.3 | *k*-means clustering

The *k*-means algorithm is a centroid-based clustering method that allocates different observations to *k* clusters so that the sum of squared distances within a cluster is minimized (Hartigan and Wong, 1979). Therefore, the algorithm requires randomly selected *k* initial cluster centres. Each input field is assigned to the nearest cluster by calculating the Euclidean distance between the data point and each cluster centre. Subsequently, the assigned points of a cluster are averaged to define a new cluster centre. These steps are repeated until none of the cluster assignments change (Hartigan and Wong, 1979; Clark *et al.*, 2018). This method was previously used by Clark *et al.* (2018) for the clustering of rainfall data over northwestern Australia. In this study, we adopt their approach and cluster monthly rainfall anomalies in the winter–spring season between 1979 and 2015 (222 months) over SEA (29-40°S, 140–154°E). The clustering region for SEA comprises parts of the states of Victoria, New South Wales and South Australia (Figure 1a). In line with Clark *et al.* (2018), the maximum value of the Silhouette Score is
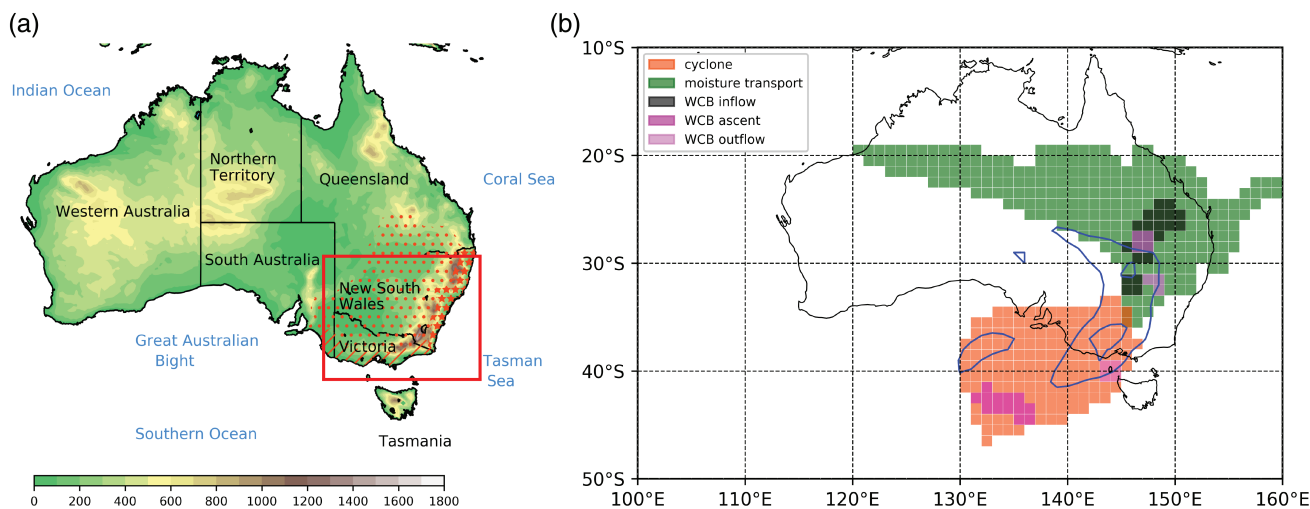
**FIGURE 1** (a) Map of Australia showing the topography (shading in m) and the clustering area (red box). Marked regions (in red) point to the three topographic drainage divisions in SEA: South East Coast Victoria (hatched), South East Coast New South Wales (stars) and Murray–Darling Basin (MDB; dotted). The topographic dataset is the 0.25°×0.25° elevation data TerrainBase from the National Center for Atmospheric Research (www.research.jisao.washington.edu/data_sets/elevation/; accessed 25 April 2020). The assignment of the regions to drainage divisions are based on the Australian Hydrological Geospatial Fabric dataset (www.bom.gov.au/water/geofabric/; accessed 25 April 2020). (b) An illustrative example that introduces the dataset of flow features (shading, different colours) based on ERA-Interim (Sprenger *et al.*, 2017) for 29 August 1992 at 1200 UTC over Australia with 6-hourly accumulated ERA-Interim rainfall (blue contours with 5 mm intervals)

used to find the physically most sensible number of clusters.

## 2.4 | Monte Carlo approach and robustness testing

In looking for a physical connection between El Niño and rainfall in SEA, one needs to know if signals in the anomalies of the composites during El Niño result by chance or if they differ substantially from the sampling dataset. A Monte Carlo method is used to test the significance of cluster composites (Scherrer *et al.*, 2006; Martius *et al.*, 2008). For each cluster, 1,000 composites of the same size are computed by randomly selecting months without replacement from the full database (June–November, 1979–2015). We consider these 1,000 randomized composites to be pure noise without any physical link. In a next step, the ENSO-based composite (cluster) is ranked in the distribution of the 1,000 randomized composites. The two types of composites should differ substantially if El Niño is changing the behaviour of selected variables (e.g., rainfall, flow features, geopotential) over SEA. If the cluster composite falls below (negative anomalies) or above (positive anomalies) a selected significance level, the anomalies are defined as statistically significant.

Additionally, we test whether the cluster composite is dominated by individual months or whether the anomalous pattern is noticeable in all months of a cluster.

The Monte Carlo approach above is repeated a second time for each cluster, but with the difference that the sampling is done with replacement from each cluster. This results in 1,000 composites which are conditioned on each cluster. It is possible that we obtain composites that consist exclusively of only one month due to the replacement after each randomly selected month from the sampling dataset. Again, the ENSO-based composite is ranked in the distribution of the 1,000 randomized composites. The interdecile range (between the 10 and 90% deciles) gives information about the statistical dispersion of the sampling dataset. The ENSO-based composite is considered as robust when the interdecile range of the 1,000 randomized composites is smaller than the ENSO-based composite.

## 2.5 | Matching of rainfall with weather systems and decomposition

In order to attribute rainfall to weather systems, we match AWAP rainfall data with derived ERA-Interim flow features. For this purpose, we downscale the flow-feature data by interpolating the data to the 0.05° rainfall grid. As cut-off lows and frontal systems are the main rain-bringing weather systems in SEA in the winter half-year (Pook *et al.*, 2006), the focus is on WCB ascent as proxy for frontal rainfall and cut-off lows. The WCB and cut-off low masks are spatially inflated to make sure that potential remote effects of the weather systems, apart from their spatial extension

identified by the algorithms, are captured. We therefore define a radius of influence of $R = 500$ km (Catto *et al.*, 2012a; Abatzoglou, 2016). The justification for this choice is outlined in Section 3.3. Daily rainfall is matched with the inflated 6-hourly masks of cut-off lows and WCBs with the condition that, in at least one of the four time steps, the mask shows the presence of a cut-off low, a WCB or both. If there is rainfall at a grid point but neither of the two weather systems, we define a fourth case for non-matched rainfall over SEA. In order to avoid the matching of drizzle to weather systems in particular along the coasts, daily rainfall amounts of less than 1 mm are ignored.

To investigate whether rainfall anomalies during El Niño can be attributed to an intensity or frequency change of precipitation associated with any of the four cases, we adjust a method which has been used in previous studies (Catto *et al.*, 2012b; Clark *et al.*, 2018). Rainfall anomalies within a cluster are decomposed into a change due to anomalous rainfall intensity changes and due to anomalous frequency of rainfall associated with a certain weather system:

$$\overline{P_{2,j}} - \overline{P_1} = \sum_{i=1}^{4} [(f_{2,i,j} - f_{1,i})P_{1,i} + (P_{2,i,j} - P_{1,i})f_{1,i} + (f_{2,i,j} - f_{1,i})(P_{2,i,j} - P_{1,i})]. \tag{1}$$

Here, $\overline{P_{2,j}}$ is the accumulated rainfall in cluster $j$ divided by the number of days in cluster $j$, and $\overline{P_1}$ is analogously the total rainfall in the winter–spring period 1979–2015 divided by the number of all days in this period. The variable $P_{2,i,j}$ is the daily mean rainfall within Cluster $j$ and $P_{1,i}$ represents the daily mean rainfall in the winter–spring period 1979–2015 associated with the matching case $i$, that is, WCB, cut-off low, both weather systems, non-matched. The frequency $f_{1,i}$ is the relative proportion of rainfall days by the matching case $i$ to the total number of days in the winter–spring season 1979–2015 and represents the climatological frequency that is used for all clusters. In contrast, the frequency $f_{2,i,j}$ is the relative proportion of rainfall days by the matching case $i$ to the total number of days in one selected cluster $j$. The first term at the right-hand side represents the change in rainfall due to a change in frequency of a specific matching case. The second term represents changes in the intensity of rainfall and the third term includes changes in both. Each term is calculated for the four matching cases $i$ and the sum of the 12 terms makes the total change in rainfall in a cluster $j$.

## 2.6 | Trajectory analysis

A set of backward trajectories is computed with the Lagrangian analysis tool LAGRANTO (Sprenger and Wernli, 2015) to investigate the origin of air masses associated with rainfall. LAGRANTO uses ERA-Interim three-dimensional wind fields at 60 model levels to calculate the 240 hr (10-day) backward trajectories. Trajectories are started 6-hourly at an equidistant grid of $60 \times 60$ km and at 17 equidistant levels between 970 and 490 hPa over SEA. The starting time of the trajectories is referred to as $t = 0$ hr. Following Sodemann *et al.* (2008), it is assumed that the relative humidity of precipitating air parcels exceeds 80% at $t = 0$ hr. In the following, we only consider those parcels which fulfil this criterion. We differentiate between backward trajectories from cut-off low and WCB rainfall by assigning the trajectories to rainfall at the nearest grid points where rainfall is matched with either of the two weather systems.

To distinguish between different trajectory pathways, the backward trajectories are clustered with the hierarchical agglomerative clustering approach by Hart *et al.* (2015) which is briefly described in the following. In this approach, we cluster the trajectories based on their horizontal position over time. Each trajectory $j$ is treated as one observation and is stored in the observation vector

$$\mathbf{W}_j = \left[ \lambda_{j,t=0}, ..., \lambda_{j,t=T}, \ \phi_{j,t=0}, ..., \phi_{j,t=T} \right], \tag{2}$$

where $\lambda(t)$ and $\phi(t)$ are the longitude and latitude position of a trajectory for a specific time $t$. Prior to the actual clustering code, all observations are stored in a data matrix $\mathbf{W}$ containing all observations each described by $N$ dimensions. Using 10-day backward trajectories with a temporal resolution of 6 hrs, each observation vector $\mathbf{W}_j$ holds $N=82$ entries. Initially, each observation vector is a cluster. Once the clustering starts, the most similar trajectory clusters are agglomerated iteratively into new cluster classes. As a measure for the similarity of two observations, we use the Euclidean distance

$$d_{j,k} = \sqrt{\sum_{n=1}^{N} \left\{ \mathbf{W}_j(n) - \mathbf{W}_k(n) \right\}^2}, \tag{3}$$

with $k$ and $m$ as indices for two trajectories whose similarity is compared. The final number of clusters is determined by an abrupt increase in the second derivative of the mean distance between successive clusters. Hart *et al.* (2015) give further details.

## 3 | RESULTS

### 3.1 | Monthly rainfall anomaly patterns for SEA

The number of clusters $k$ is varied between 2 and 7. For each case, the average silhouette score is calculated (not
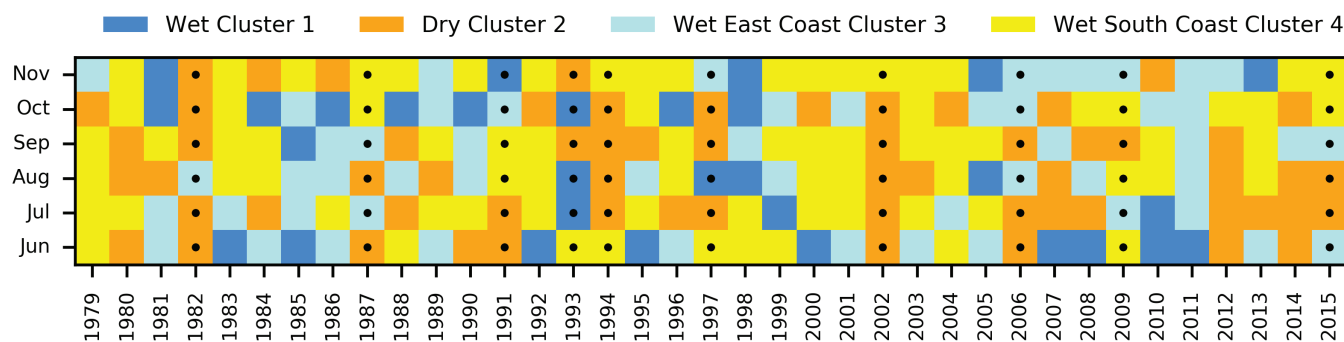
**FIGURE 2** The resulting assignment of monthly rainfall anomalies in the winter–spring season (1979–2015) in SEA to the four clusters based on the *k*-means clustering. El Niño months are marked with a black point

shown). With an increasing number of clusters, the silhouette score also increases and peaks at four clusters before it falls. Consequently, four clusters is a suitable choice. More clusters leads to a split of a cluster into two nearly similar rainfall anomaly patterns. Fewer clusters misses one of the key rainfall anomaly patterns. Taking the ENSO state classification by Pepler *et al.* (2014) and by the Bureau of Meteorology (http://www.bom.gov.au/climate/enso/enlist; accessed 25 April 2020), subsets of the full clusters are generated that purely contain winter–spring months in El Niño years. Ten El Niño events occurred in the selected period between 1979 and 2015: 1982, 1987, 1991, 1993, 1994, 1997, 2002, 2006, 2009, 2015. These subsets of clusters containing only El Niño-affected months are referred to as El Niño clusters in the following. We now focus on the characteristics of the resulting rainfall anomaly clusters over SEA and present changes in the patterns and in the occurrence of the full clusters and the El Niño clusters (Figures 2 and 3).

The first full cluster is characterised by significant and robust above-average monthly rainfall over SEA (Figure 3a). The highest anomalies of more than $100 \, mm \cdot month^{-1}$ are found west of the Great Dividing Range (a mountain range stretching parallel to the southeast coast; Figure 1a). Full Cluster 1 contains the fewest months (in total: 30 months), which corresponds to a percentage of only 13.5% of all months in the winter–spring season between 1979 and 2015 (Table 1). El Niño Cluster 1 is the subset of El Niño-affected months in full Cluster 1 and comprises five months that occurred in only three of the ten El Niño years (Figure 2). In El Niño Cluster 1 (Figure 3b), positive rainfall anomalies are greater than climatology over southern New South Wales and Victoria (Figure 3a,b). Over Queensland and northern New South Wales, rainfall is lower in the El Niño Cluster 1. The lower observed above-average rainfall pattern during El Niño is illustrated by a smaller percentage of El Niño months that fall into Cluster 1 (8.3%) compared to all months in full Cluster 1. El Niño Cluster 1 is further referred to as

"wet Cluster 1". The second full cluster includes around 27.9% of all months in the winter–spring season from 1979 to 2015 (Table 1) and shows significant and robust below-average monthly rainfall with anomalies of up to $-100 \, mm \cdot month^{-1}$ in coastal areas (Figure 3c). El Niño Cluster 2 includes nearly 50% of all El Niño months (Table 1) pointing to a relative change in the appearance of around 73% from the full cluster to the El Niño cluster. During El Niño, in most areas, rainfall is slightly less than for all months in this cluster (Figure 3d). El Niño Cluster 2 is further referred to as dry Cluster 2. Full Cluster 3 comprises 23.9% of all winter–spring months from the period 1979–2015 (Table 1) and is characterised by significant and robust positive rainfall anomalies along the East Coast and significant and robust negative rainfall anomalies along the South Coast (Figure 3e). When focusing on El Niño, the number of months falls to 12 and the anomalies along the South Coast and northern East Coast increase in magnitude (Table 1; Figure 3f). Cluster 3 occurs less often during El Niño with a relative occurrence change of around 16% compared to the full Cluster 3. Rainfall anomalies along the East Coast are statistically significant but not robust in the El Niño cluster (Figure 3f). The *k*-means clustering with five clusters demonstrates that an additional cluster would result from the split of Cluster 3 with positive anomalies in different regions along the East Coast. This points to a high spatial variability of rainfall anomalies within this cluster and explains why the anomalies are significant but not robust. We will further use the term "wet East Coast Cluster 3" for El Niño Cluster 3. The fourth Cluster is the reversed pattern of Cluster 3 and comprises with 34.7% the greatest fraction of months (Figure 3g,h and Table 1). Significant and robust positive (negative) rainfall anomalies along the South Coast (East Coast) characterise the monthly rainfall composite of Cluster 4 (Figure 3g). During El Niño, the rainfall anomaly pattern shows drier conditions compared to the full Cluster 4 (Figure 3h). The reduced percentage of months in El Niño Cluster 4 (23.2%) points to the fact that this pattern is observed slightly
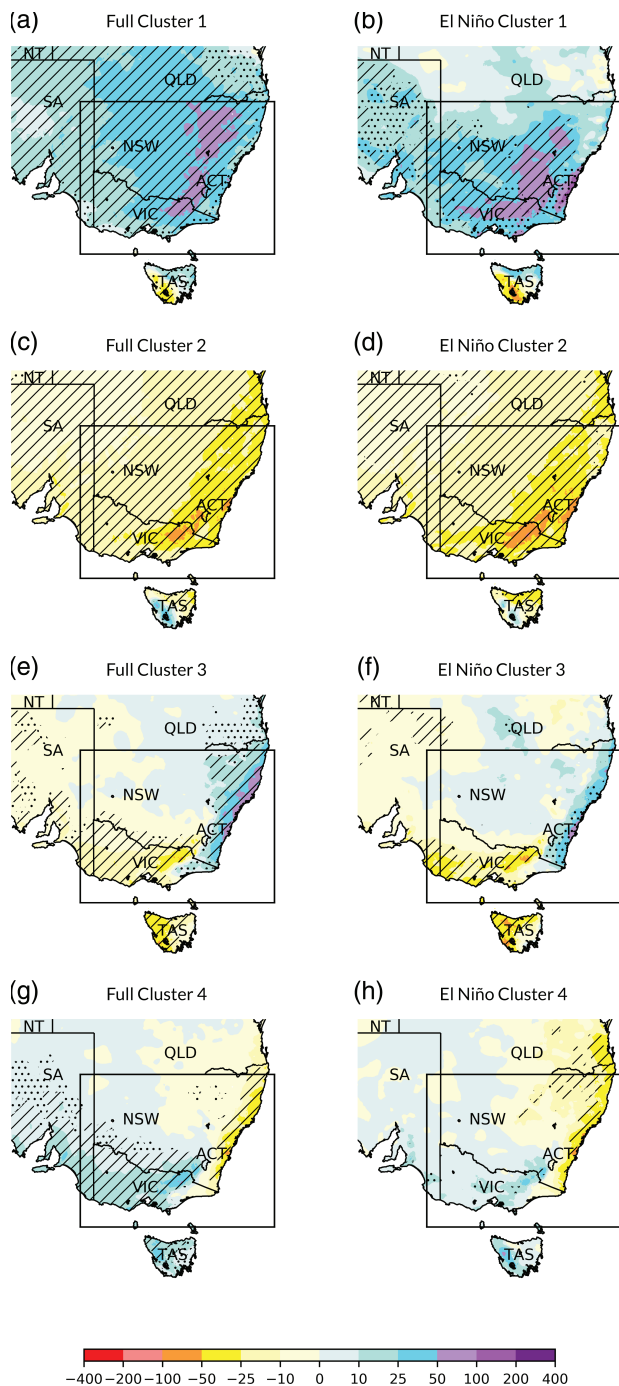
**FIGURE 3** Monthly rainfall anomaly patterns (shading in mm) as a result of clustering monthly rainfall anomalies in the winter–spring season in the period 1979–2015 over SEA for (a, c, e, g) the full clusters and (b, d, f, h) the El Niño subset of clusters. The anomaly patterns are shown for the extended southeastern Australian region including a part of the states Victoria (VIC), New South Wales (NSW), Australian Capital Territory (ACT), South Australia (SA), Queensland (QLD), Tasmania (TAS) and Northern Territory (NT). The black box marks the clustering area. Statistically significant rainfall anomalies that exceed the upper 2%iles or fall below the lower 2%iles are dotted. Anomalies which are additionally robust within the cluster are hatched. Monthly rainfall anomalies of –1 to 1 mm are not shaded

less often during El Niño than in the full period from 1979–2015. El Niño Cluster 4 is further referred to as "wet South Coast Cluster 4". For all clusters, the distribution of months within both cluster sets highlights that there are no clear preferred months in which a specific rainfall anomaly pattern occurs (Table 1).

Although ENSO seems to be the dominant driver of rainfall variability, we further looked at the behaviour of monthly SAM values (Marshall, 2003) and IOD values (Hameed and Yamagata, 2003) within the clusters. In essence, we find no striking differences in the distribution of monthly IOD values between the four rainfall clusters, neither in the full nor in the El Niño subsets (not shown). Although the distribution of SAM values varies between the clusters, the differences in the distribution between the full and El Niño cluster within an individual rainfall cluster are not statistically significant (not shown).

## 3.2 | Weather systems in the Australian region

This section focuses on the variability of weather system occurrences. We first present the climatology and continue with a discussion of large-scale anomaly patterns and weather system occurrence anomalies in the four El Niño clusters.

### 3.2.1 | Climatology

Climatologies of weather systems during the Australian winter–spring season (JJASON) are calculated for the reference period 1979–2015 (Figure 4). In the Australian region, cut-off lows predominantly occur between 30° and 50°S (dashed blue contour in Figure 4a). Enhanced moisture fluxes show their highest occurrence over the Tasman Sea and southwest of Australia (solid green contour). With focus on Australia, atmospheric blocking frequencies (shading) increase poleward and indicate a maximum of up to 24% between 40° and 60°S in the storm track area of the Southern Hemisphere (Trenberth, 1991). A clear occurrence maximum of cyclones is visible along the storm track region to the south of Australia (Figure 4b, shading). Apart from this maximum, further cyclone maxima are located over the Tasman Sea and over northwestern Australia (roughly 125°E, 20°S) with occurrence frequencies of up to 12%. Most of the WCB activity is concentrated southeast and southwest of Australia (Figure 4b). WCB inflow dominates along 35°S with a maximum climatological frequency east of Australia over the Coral Sea (solid blue contour). The WCB ascent, which represents the main ascending and precipitating part of the WCB, is mainly

**TABLE 1** Main characteristics of the winter–spring monthly rainfall anomaly clusters for the period 1979–2015 and the reduced sample based on ten El Niño events.

| Cluster | Pattern | Months | Percentage | J | J | A | S | O | N |
|---|---|---|---|---|---|---|---|---|---|
| Full Cluster 1 | Wet SEA | 30 | 13.5 % | 5 | 8 | 1 | 4 | 3 | 9 |
| Full Cluster 2 | Dry SEA | 62 | 27.9 % | 5 | 10 | 12 | 11 | 15 | 9 |
| Full Cluster 3 | Wet East Coast, dry South Coast | 53 | 23.9 % | 9 | 9 | 8 | 10 | 7 | 10 |
| Full Cluster 4 | Dry East Coast, wet South Coast | 77 | 34.7 % | 18 | 10 | 16 | 12 | 12 | 9 |
| Sum (full) | | 222 | 100 % | 37 | 37 | 37 | 37 | 37 | 37 |
| El Niño Cluster 1 | Wet SEA | 5 | 8.3 % | 1 | 1 | 0 | 2 | 1 | 0 |
| El Niño Cluster 2 | Dry SEA | 29 | 48.3 % | 2 | 4 | 7 | 4 | 7 | 5 |
| El Niño Cluster 3 | Wet East Coast, dry South Coast | 12 | 20.0 % | 3 | 2 | 2 | 2 | 2 | 1 |
| El Niño Cluster 4 | Dry East Coast, wet South Coast | 14 | 23.2 % | 4 | 3 | 1 | 2 | 0 | 4 |
| Sum (El Niño) | | 60 | 100 % | 10 | 10 | 10 | 10 | 10 | 10 |

*Note:* The upper four rows characterise the clusters based on the full time period; the lower four rows show information from the El Niño subset of clusters. The description of the rainfall patterns is with regard to the cluster mean monthly rainfall anomalies. The third column gives the absolute number of months within each cluster. The fourth column shows (upper) the percentage number of months out of all winter–spring months 1979–2015 that are associated with the indicated cluster, and (lower) the percentage number of El Niño months out of all winter–spring El Niño months in each cluster. Columns 5–10 illustrate the composition of the clusters by months in the winter–spring season.

observed south of the inflow region maxima and points to the fact that most WCBs ascend polewards (Madonna *et al.*, 2014). The WCB ascent occurs over SEA, the Tasman Sea, the Coral Sea and the Southern Ocean (dashed orange contour). A maximum of the WCB ascent over the Tasman Sea overlaps with a cyclone occurrence maximum, highlighting the relationship and the simultaneous appearance of WCBs and extratropical cyclones. The WCB outflow in the upper troposphere mostly occurs in the New Zealand region and far south of Western Australia (solid green contour).

### 3.2.2 | Changes in the occurrence of weather systems during El Niño

Next, we investigate the modulation of weather system occurrence frequencies within El Niño clusters. Therefore, we compute monthly anomalies relative to the monthly climatology based on the period 1979–2015. All monthly anomalies within a cluster are averaged and tested for statistical significance and robustness using the Monte Carlo approach to ensure that statistically significant anomalies are not dominated by individual months within a cluster.

Anomalously high geopotential southeast of Australia dominates the large-scale atmospheric circulation in wet Cluster 1 (Figure 5a,b). Enhanced atmospheric blocking collocated with the positive geopotential anomalies south and east of Australia indicates a quasi-stationary wave pattern around Australia, possibly resulting from recurrent anticyclonic wave breaking. Negative geopotential

anomalies are situated over West Australia and stretch to parts of Southern Australia. The occurrence frequency of rain-bringing weather systems is significantly enhanced over SEA (Figure 5a). Cut-off lows occur twice as frequently as climatologically along the southern East Coast of Australia (not shown). The frequency of WCB ascent is increased across SEA and to the north of the enhanced cut-off low frequency. Its collocation with positive frequency anomalies of enhanced moisture fluxes indicates that WCBs ascend in a moist northwesterly flow and ahead of cut-off low systems.

Positive geopotential height anomalies cover most parts of Australia in dry Cluster 2 (Figure 5c,d). The structure with its centre over the Great Australian Bight deviates from the climatological mean by more than $25 \, \text{m}^2 \cdot \text{s}^{-2}$. Similar to wet Cluster 1, an enhanced frequency of blocking is observed near the centre of the positive geopotential anomaly structure (Figure 5c). There is a clear reduction of weather system frequencies (cut-off lows, WCBs, moisture fluxes, cyclones) around Australia in particular over eastern Australia and the Tasman Sea (Figure 5d).

In wet East Coast Cluster 3, strong positive geopotential anomalies of up to $35 \, \text{m}^2 \cdot \text{s}^{-2}$ characterise the large-scale pattern and point to anomalous high pressure south of Australia (Figure 5e,f). An enhanced frequency of blocking is observed within the positive geopotential anomalies around 120°E and around 145°E and 175°E (Figure 5e). In conjunction with negative frequency anomalies of blocking over the Tasman Sea along 35°S, this suggests a poleward shift of blocking in wet East
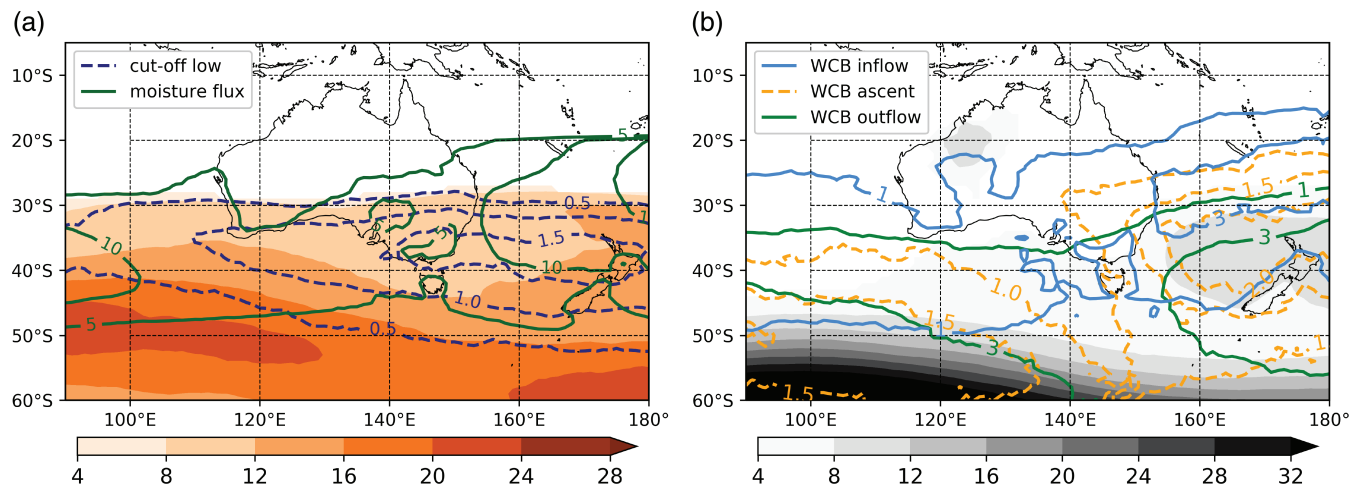
**FIGURE 4** Australian winter–spring climatology of weather systems based on the reference period 1979–2015. (a) shows climatologies of cut-off lows averaged between 315 and 320 K levels (dashed blue contours every 0.5%, starting at 0.5%), moisture flux (solid green contours every 5%, starting at 5%) and atmospheric blocking (colour shading, every 4%). (b) shows climatologies of WCB inflow (solid blue contours at 1 and 3%), WCB ascent dashed orange contours every 0.5% starting at 1%), WCB outflow (solid green contours at 1% and 3%) and cyclones (grey shading, every 4%). The values represent the percentage occurrence of 6-hourly time steps from ERA-Interim

Coast Cluster 3 (Figure 5f). Cut-off lows predominantly occur more frequently over SEA and over the Tasman Sea (Figure 5e). A more detailed view indicates that cut-off lows are twice as frequent around 35°S during El Niño (not shown).

The anomalous circulation over Australia in wet South Coast Cluster 4 markedly differs from the patterns in the other clusters (Figure 5g,h). Well-pronounced negative geopotential anomalies of less than −35 $m^2 \cdot s^{-2}$ south of Australia dominate the large-scale pattern. There are no significant positive anomalies in weather system frequency over SEA (Figure 5g). Cut-off lows, which usually develop during blocking to the southeast of Australia, show a significant decline in frequency over the Tasman Sea (Figure 5h). In addition, the cyclone and WCB outflow frequencies are also significantly reduced east of Australia.

## 3.3 | Contribution of weather systems to rainfall during El Niño

Although the results in Section 3.2.2 demonstrate that positive (negative) rainfall anomalies are mostly related to an increased (decreased) frequency of weather systems around Australia, they say little about the origin of rainfall, in particular for individual rainfall events. For this reason, we now match daily rainfall events with cut-off lows and WCBs and assess the percentage of total rainfall that can be attributed to one of these weather systems in the El Niño clusters (Figure 6). This method shows the importance of a weather system for the total rainfall, but it does not reveal whether this is due to an intensity change

or due to a frequency change of the respective weather system. Therefore, we use the decomposition method of Clark *et al.* (2018) to calculate the changes in rainfall characteristics during El Niño relative to the winter–spring climatology period 1979–2015 for each cluster and grid point. We calculated the spatial mean over three drainage division areas over SEA from the Australian Hydrological Geospatial Fabric to make quantitative statements of the results (Figure 1a): South East Coast Victoria (in short, South Coast), South East Coast New South Wales (in short, East Coast) and the Murray–Darling Basin (MDB).

In wet Cluster 1, WCBs are the main contributors to rainfall inland of SEA and explain locally more than 50% of the total cluster rainfall (Figure 6a). In the MDB which covers the inland regions of SEA up to southern parts of Queensland, 36% of the total rainfall can be assigned to WCBs (Figure 6b). A combined occurrence of cut-off lows and WCBs contributes 32% to the total rainfall. The decomposition shows that above-average rainfall in this area results from an enhanced frequency of WCB rainfall and an increased occurrence of the combination of cut-off lows and WCBs compared to climatology (Figure 7a). Along the East Coast, about 80% of the rainfall is dominated by a co-occurrence of cut-off lows and WCBs (Figure 6a). The co-occurrence contributes 40% to the total rainfall to the East Coast drainage division (Figure 6b). This is mostly due a frequency change (Figure 7a). WCBs in combination with cut-off lows bring most of the rainfall to the South Coast in wet Cluster 1 (Figure 6a). In the South Coast drainage division, 30% of the total rainfall can be explained by WCBs and a further 28% by the co-occurrence with cut-off lows (Figure 6b). That the positive anomalies
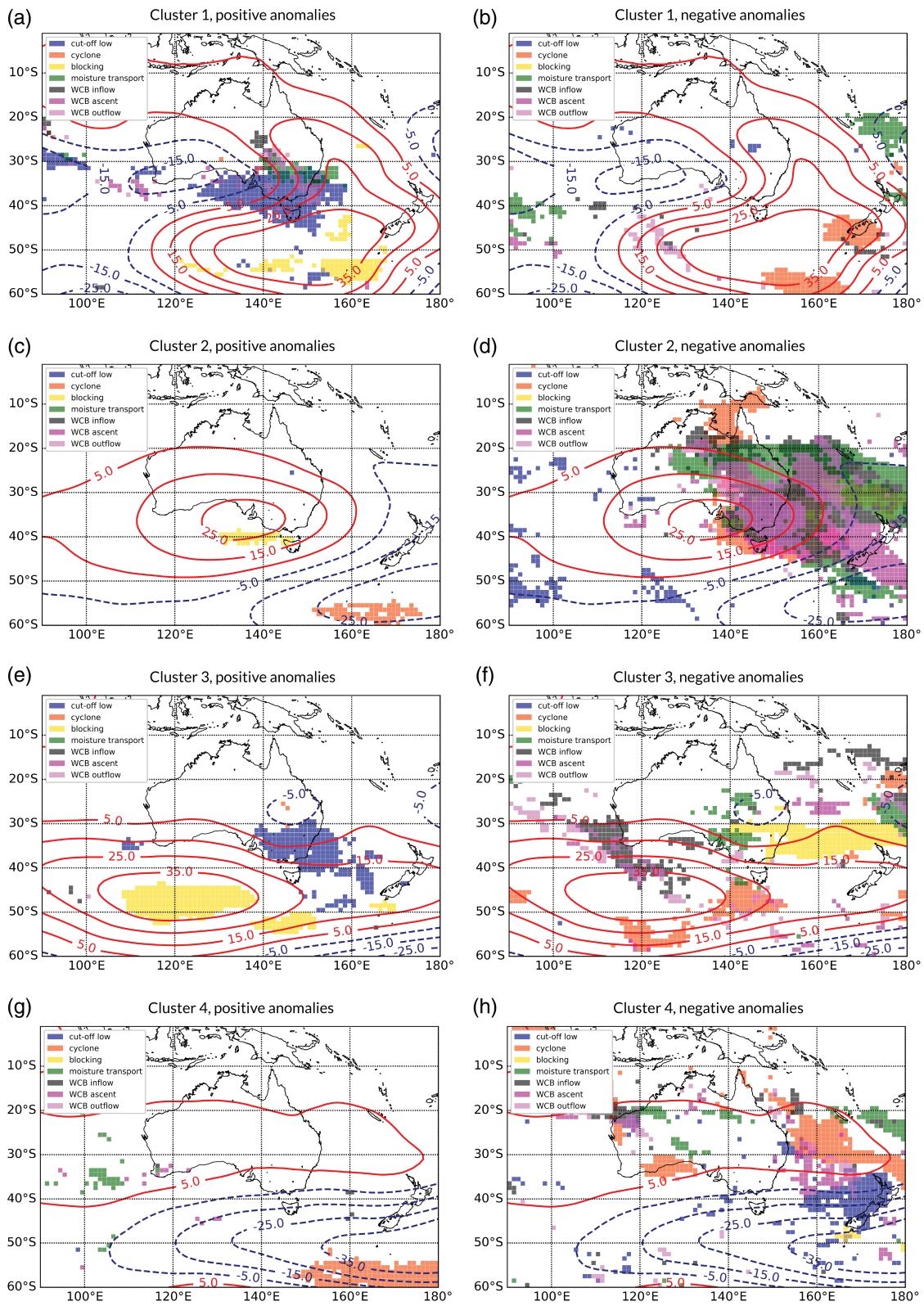
**FIGURE 5** (a, c, e, g) Positive and (b, d, f, h) negative frequency anomalies of weather systems (shading) and mean geopotential anomalies for the El Niño clusters: (a, b) wet Cluster 1, (c, d) dry Cluster 2, (e, f) wet East Coast Cluster 3 and (g, h) wet South Coast Cluster 4. Only robust (upper 90%iles and lower 10%iles) and significant (upper 98%iles and lower 2%iles) frequency anomalies of the Monte Carlo composites are displayed in the specific colour. As an example, the filled blue area in (a) points to a significant increase of cut-off-low frequency that is robust within the cluster. The contour lines indicate geopotential anomalies ($m^2 \cdot s^{-2}$) at 500 hPa: positive anomalies in solid red and negative anomalies in dashed blue lines

**FIGURE 6** The results of matching daily rainfall with cut-off lows and WCBs in SEA for the El Niño clusters. (a, c, e, g) show the dominant contributor to rainfall for each grid point (colour shading). Colour intensities indicate the percentage amount of the total rainfall within a cluster that is explained by the dominant contributor. Black lines show the location of the South East Coast drainage division in Victoria (South Coast), New South Wales (East Coast) and the Murray–Darling Basin (MDB). (b, d, f, h) show bar plots indicating the percentage of total cluster rainfall that can be attributed to WCBs, cut-off lows, both, or none of these
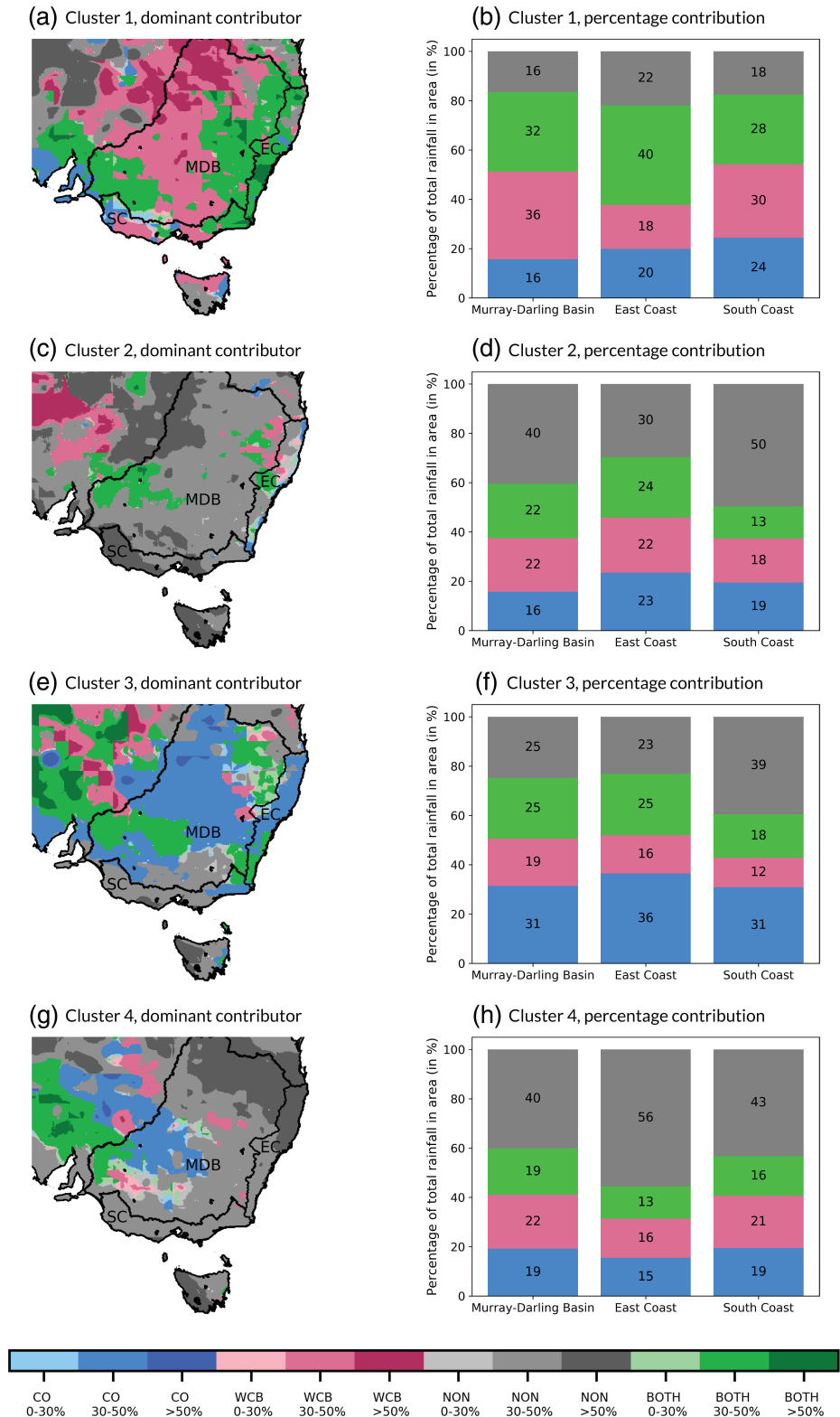


along the South Coast result from an increased frequency of WCBs, cut-off lows and rainfall of both (Figure 7a) highlights the importance of these weather systems in general along the South Coast.

A large percentage of total rainfall cannot be assigned to cut-off lows or WCBs in SEA in dry Cluster 2 (Figure 6c).

In the MDB, 40% of the total cluster rainfall cannot be explained by cut-off lows and WCBs (Figure 6d). WCB rainfall and rainfall related to both weather systems each contributes 22%. The negative rainfall anomalies in the MDB in dry Cluster 2 are caused by decreased frequencies of the rainfall from cut-off lows and WCBs compared
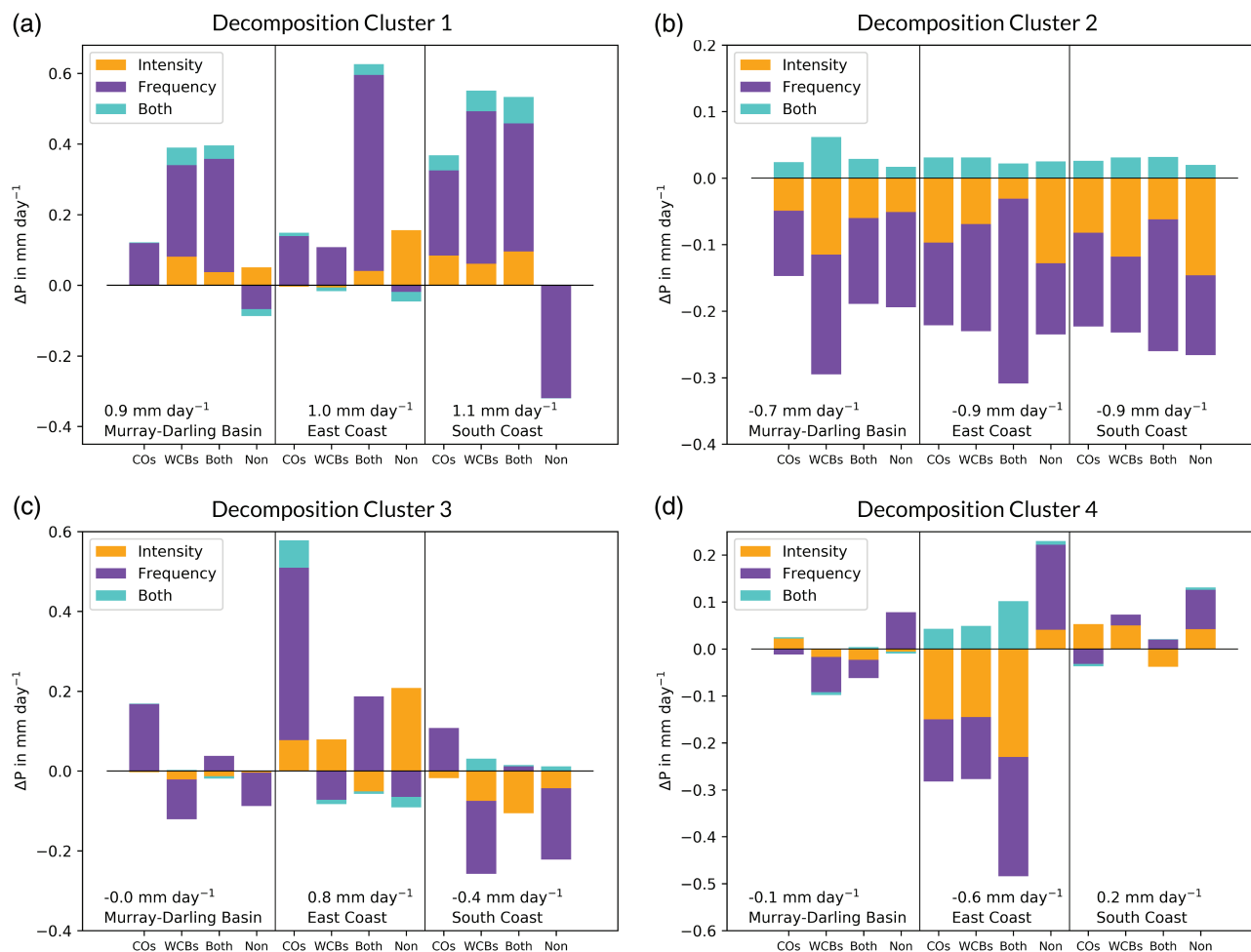
**FIGURE 7**   Results of the decomposition of rainfall during El Niño in the rainfall clusters over SEA. The bars show the contribution of changes in intensity and frequency of rainfall to the total rainfall anomalies in mm·day$^{-1}$ in each of the drainage divisions. As the decomposition is made for each matching case separately, four stacked bars (four matching cases) represent the total change of rainfall in each drainage division. As an example, in (a) there is increased WCB-related rainfall in the Murray–Darling Basin in Cluster 1 (+0.4 mm·day$^{-1}$) compared to the climatology, with a change in the frequency that contributes around +0.25 mm·day$^{-1}$ to the WCB rainfall change. The total rainfall change is given at the bottom of each plot

to climatology with the highest declines in WCB rainfall (Figure 7b). Along the East Coast, the main contributor to rainfall strongly varies locally (Figure 6c). With a focus on the East Coast drainage division, 30% of the total rainfall is not related to the considered weather systems and the remaining 70% are equally split between cut-off lows and WCBs (Figure 6d). The rainfall decline along the East Coast is a result of less frequent rainfall related to WCBs and cut-off lows and less intense non-weather-system rainfall events (Figure 7b). Half of the total rainfall along the South Coast results from rainfall events that are not connected to cut-off lows and WCBs (Figure 6d). The decomposition demonstrates that especially a reduced frequency of cut-off low and WCB rainfall and a strong decrease in the intensity of non-weather-system related rainfall explain below-average rainfall along the South Coast drainage division in dry Cluster 2 (Figure 7b).

A major part of SEA receives a high percentage of total rainfall from cut-off lows in the wet East Coast Cluster 3 during El Niño (Figure 6e). Cut-off lows are the main contributors and bring 31% of the total rainfall in the MDB (Figure 6f). Although WCB and unmatched rainfall occur less frequently in this area, the total rainfall anomaly is zero due to the compensation by an increased frequency of cut-off-low rainfall compared to climatology (Figure 7c). With a percentage of 36%, cut-off lows are also the main contributors to rainfall along the East Coast, followed by rainfall related to both contributing 25% to the total rainfall (Figure 6e,f). The strongly increased frequency of cut-off lows is especially important for the pronounced positive rainfall anomalies in the East Coast drainage division (Figure 7c). In contrast to the previous drainage divisions, the majority of the total rainfall along the South Coast is not related to cut-off lows or WCBs

(Figure 6e,f). Still, the decomposition reveals that negative rainfall anomalies in the South Coast drainage division are mainly connected with a decreased frequency of WCB rainfall and rainfall that is not related to either cut-off lows or WCBs (Figure 7c).

In wet South Coast Cluster 4, a high proportion of rainfall in SEA is not related to cut-off lows or WCBs (Figure 6g). The main contributors to rainfall in the MDB vary spatially, but rainfall not related to either of the two weather systems shows the highest percentage contribution of 40% (Figure 6g,h). Near-normal rainfall in the MDB results from the combination of a decreased frequency of WCB and cut-off-low rainfall and an increased frequency of rainfall that is not related to these weather systems (Figure 7d). Along the East Coast, more than half of the total rainfall is not related to the weather systems considered here (Figure 6h). The rainfall decline in the East Coast drainage division is related to a strong decrease in the frequency and intensity of rainfall from cut-off lows and WCBs compared to climatology (Figure 7d). Of the total rainfall along the South Coast, 43% is not connected with WCBs and cut-off lows (Figure 6h). Slightly above-average rainfall in the South Coast drainage division results from more intense cut-off low and WCB rainfall and more frequent rainfall not associated with either cut-off lows or WCBs (Figure 7d).

We tested the sensitivity of this radius of influence by comparing the matching results at different radii (250, 750, and 1,000 km). As the radius increases, a larger proportion of rainfall is matched with both weather systems, cut-off lows and WCBs. In contrast, the proportion of rainfall that is not related to the two weather systems decreases with increasing radius as a larger area is assigned to the weather systems. However, the pure cut-off-low and WCB percentages (Figure 6b, d, f, h) do not change much with increasing radius, so that the choice of $R = 500$ km seems pragmatic and reasonable.

## 3.4 | Origin of air masses during El Niño rainfall

Backward trajectories that end up over SEA on wet days during El Niño are calculated. These trajectories provide insights into typical moisture pathways. Each trajectory is assigned to the closest grid point on the rainfall grid. Since daily rainfall at each grid point is matched with cut-off lows or WCBs, all trajectories are split into the four selected cases, that is, WCB, cut-off low, both and neither. Here, we only focus on the backward trajectories for cut-off low and WCB rainfall separately, as backward trajectories of rainfall related to both cut-off lows and WCBs, do not yield additional pathways and seem to represent a

mixture of the cut-off low and WCB pathways. A clustering algorithm by Hart *et al.* (2015) is used to distinguish between the different pathways. The most physically sensible number of trajectory clusters for cut-off lows and WCBs for all El Niño clusters is three, except for cut-off lows in wet Cluster 1 where the method indicates four clusters. For consistency, we choose three trajectory clusters for all rainfall clusters. Specific humidity is tracked along the trajectories which allows us to identify moisture source and sink regions. In the following, we will first describe the pathway of air masses that end in cut-off-low precipitation, and subsequently continue with the pathway connected to WCB rainfall.

In wet Cluster 1, 51% of trajectories that are involved in cut-off-low rainfall over SEA originate from the remote inland area of Australia and reach SEA from the northwest (Figure 8a). This pathway for cut-off-low rainfall does not exist in the other clusters and hints to a connection with the increase in frequency and intensity of cut-off-low rainfall especially along the South Coast. There is a further pathway with around 30% of all trajectories from the Tasman Sea. Air parcels move anticyclonically towards SEA and reach the cut-off low at its northeastern flank, where they are possibly effectively lifted. These trajectories spend most of their time over maritime regions where they continuously moisten. A third pathway emerges from the Southern Ocean, but only 19.2% of the trajectories fall into this group. In dry Cluster 2, around 56% of air parcels that end up in cut-off-low rainfall are already over SEA 5 days prior to rainfall (Figure 8c). The anticyclonic pathway over New South Wales suggests a southward movement at the front side to the east of cut-off lows. Further pathways originate from the Southern Ocean where air parcels continuously pick up moisture on their way to SEA. In comparison to wet Cluster 1, there is no trajectory cluster that includes the anticyclonic and wet pathway from the Tasman Sea. More than two thirds of trajectories in wet East Coast Cluster 3 are located at the South Coast of Victoria 5 days prior to cut-off-low rainfall (Figure 8e). Air parcels that end up in rainfall over SEA follow an anticyclonic pathway along the East Coast over the Tasman Sea and enter the continent at the northeastern border of New South Wales. In a second pathway, air parcels start over the Southern Ocean southwest of Australia and also turn anticyclonically to SEA where they enter the continent at the southeastern border of New South Wales. Less than 10% of all trajectories originate from 70°E over the Southern Ocean and air parcels move directly within the westerly wind belt region towards SEA. In wet South Coast Cluster 4, around 44% of all trajectories that end up in cut-off-low rainfall are located over the Tasman Sea 5 days prior to rainfall (Figure 8g). Starting with low moisture content, the air parcels rapidly moisten while they turn
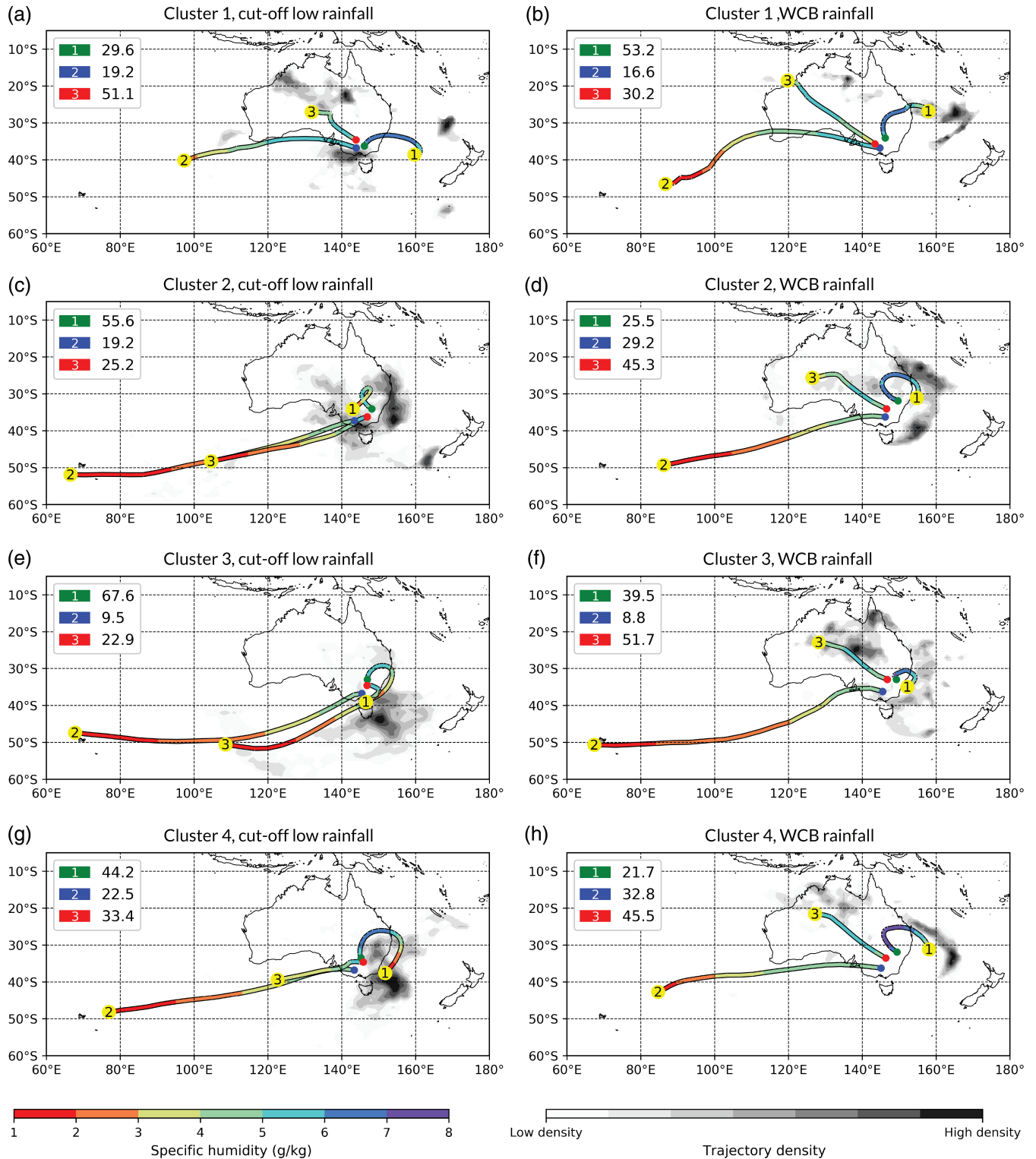
**FIGURE 8** Cluster-median backward trajectories of (a, c, e, g) cut-off-low rainfall and (b, d, f, h) WCB rainfall in the clustering box over SEA during El Niño. The total trajectory density (grey shading) for all trajectories at $t = -120$ hr is normalized and shown in 0.1 steps between 0.3 and 1.0. Each cluster-median backward trajectory shows the mean pathway in the last 5 days before the rainfall. The density and the median pathway are not necessarily collocated due to the inter-cluster variance. Coloured shading illustrates the cluster-median specific humidity $(g \cdot kg^{-1})$ along the pathway. The legend in the upper left corner of the plot gives information about the percentage of all backward trajectories that fall within a particular trajectory cluster. Coloured points at $t = 0$ hr of the cluster-median trajectories help to assign the percentage values to the respective trajectory. Yellow points at the trajectories mark the time $t = -120$ hr that is assigned to the density of trajectories (shading)

anticyclonically over the Tasman Sea towards SEA. They enter the continent at 25°S and reach SEA from the north. Two further pathways originate from the Southern Ocean.

We now focus on WCB rainfall backward trajectories. In wet Cluster 1, the majority of trajectories ending up in WCB rainfall originate from the Coral Sea and reach SEA from the north (Figure 8b). Starting with a high amount of moisture, they continuously moisten on their anticyclonic pathway towards SEA. Another pathway reaches SEA straight from the northwest coast of Western Australia. Although we see a similar pathway from the northwest in other clusters, the air parcels are located on the northwesternmost point in Cluster 1 around 5 days prior to rainfall. A third pathway points to air masses that originate from the Southern Ocean and flow cyclonically along the South Coast of Australia to SEA. In dry Cluster 2, air masses originate mostly from the remote inland area of Australia during WCB rainfall in SEA (Figure 8d). Around 30% of WCB backward trajectories point to the Southern Ocean as the source region. In contrast to wet Cluster 1, only 25% of air parcels that end up in WCB rainfall come from the Tasman Sea. More than half of all backward trajectories of WCB rainfall show a pathway from the remote inland of Australia in wet East Coast Cluster 3 (Figure 8f). Around 40% of the air parcels that end up in WCB rainfall originate from the Tasman Sea and move anticyclonically towards SEA with a noticeably higher content of moisture (over $7 \, \text{g} \cdot \text{kg}^{-1}$) in comparison to the air parcels from the inland areas of Australia. The third pathway represents less than 10% of the backward trajectories that come from the Southern Ocean. In wet South Coast Cluster 4, 45.5% of all backward trajectories of WCB rainfall have their origin 5 days prior to rainfall over northwest Australia (Figure 8h). Air parcels connected to this pathway enter SEA from the northwest and end up in rainfall over central SEA. Around a third of all air parcels move from the Southern Ocean in particular towards the southern part of SEA. Only 22% of all WCB rainfall air parcels come from the Tasman Sea, where they rapidly moisten during their anticyclonic pathway towards SEA.

## 4 | DISCUSSION

Based on the *k*-means clustering of monthly rainfall anomalies, we find four rainfall anomaly patterns in the winter–spring season (JJASON) in SEA in the period 1979–2015: wet SEA (Cluster 1), dry SEA (Cluster 2), wet East Coast (Cluster 3) and wet South Coast (Cluster 4). Ten El Niño years within the selected period are chosen to focus on rainfall variability during El Niño. The cluster containing most of the El Niño months is dry Cluster 2, which is characterised by below-average rainfall in SEA

and represents the well-known average impact of El Niño on rainfall in SEA (Risbey *et al.*, 2009b). However, the five months in wet Cluster 1 exhibit above-average rainfall during El Niño and underscore the notion that El Niño does not necessarily lead to drought conditions over SEA (Kane, 1997). Qualitatively, the resulting monthly rainfall anomaly clusters show similarities with the results of Risbey *et al.* (2009b). In their study, the clustering of Australian winter rainfall (JJA) in the period 1960–2004 yields five clusters that also differentiate between rainfall anomalies that spread over the continent and rainfall anomalies that are concentrated along the coasts. We investigate weather system frequencies during El Niño, match daily rainfall with cut-off lows and WCBs, and find different pathways of air masses that end up in rainfall.

Wet Cluster 1 is characterised by above-average rainfall. The rainfall pattern is known and has been discussed in several studies mostly in connection with the strong El Niño of 1997 which led to near-average annual rainfall in Australia (e.g., Brown *et al.*, 2009; van Rensch *et al.*, 2019). We find increased blocking southeast of Australia in combination with an enhanced frequency of cut-off lows, WCBs and enhanced moisture fluxes over SEA during wet months. This is partly in accordance with the results of Risbey *et al.* (2009a), who find in their "wet Australia" rainfall pattern a favoured region of development of cut-off lows due to blocking southeast of the continent. Risbey *et al.* (2009a) further mention that the variability in rainfall from frontal systems seems to be regulated by extratropical processes and not primarily by tropical processes like ENSO. The results of this study point to the importance of WCBs, which are very closely related to fronts, as sources of rainfall in wet Cluster 1. An increased frequency of WCB rainfall and rainfall related to WCBs and cut-off lows lead to the positive rainfall anomalies over SEA in wet Cluster 1. This result is in a contrast to the finding of Brown *et al.* (2009), who attribute wet conditions during El Niño to an enhanced intensity but not an increased frequency of cut-off lows in northwestern Victoria. These differences are probably due to the limited consideration of only eight stations in northwestern Victoria, a different identification method of cut-off lows and, most importantly, the different observation period (April–October) and temporal data aggregation in Brown *et al.* (2009). Even though most of the months in the selected El Niño years of Brown *et al.* (2009) fall in our dry Cluster 2, there is significant rainfall variability between the months within the same El Niño years that can distort important signals over a long period. The trajectory analysis highlights the origin of air parcels from the Coral Sea and the northwest coast of Australia that end up in WCB rainfall in wet Cluster 1. The unexpected northwest Australian pathway indicates the importance of tropical air masses for rainfall during

El Niño. Contrary to what might be expected, the trajectories collect considerable moisture from the northwest coast before moving over the dry interior of Australia. Northwest cloudbands develop near the northwest coast of Australia mostly in winter, extend southeastward and, in conjunction with fronts, bring rainfall to SEA (Tapp and Barrell, 1984; Wright, 1989; Verdon and Franks, 2005). An anomalous high-amplitude trough off the coast of Western Australia and anomalous anticyclonic flow over north and east Australia are conditions that favour the development of northwest cloudbands (Tapp and Barrell, 1984). These conditions are also present in wet Cluster 1 and support the hypothesis that the pathway from the northwest coast of Australia is linked to the presence of northwest cloudbands which are in turn associated with WCBs. The pathway from the Coral Sea that is connected with the warm, unstable and heavily moistened air masses over the North Tasman Sea (Short, 2020) has already been linked to extreme rainfall events of cut-off lows, i.e. during the 1997 El Niño event (McIntosh et al., 2007; Brown et al., 2009; McIntosh et al., 2012). The pathway from the Coral Sea is not found in other clusters and seems to be a key pathway for the transport of moisture to SEA during wet months. This links to the findings of van Rensch et al. (2015) and van Rensch et al. (2019), who find a connection to high SSTs northeast of Australia and the unusually high rainfall amounts during El Niño in 1997.

Dry Cluster 2 is characterised by below-average rainfall in SEA. This is the known average effect of El Niño especially during the winter-spring season (Brown et al., 2009; Risbey et al., 2009b; Cai et al., 2010). We find that the increased frequency of blocking collocated with an anomalous anticyclone at 140°E leads to the suppression of weather system activity (cut-off lows, WCBs, extratropical cyclones, moisture fluxes) leading to drier-than-normal conditions over SEA. The anticyclonic anomaly is likely related to a Rossby wave train emerging from the tropical Indian Ocean (not shown). This is in line with the average pattern during El Niño found in Cai et al. (2011). In contrast to wet Cluster 1, there is an anomalous high percentage of rainfall that is neither related to WCBs nor to cut-off lows, with a high decline in intensity and frequency of rainfall in general. In line with the "dry Australia" pattern in Risbey et al. (2009a), low blocking activity over the Tasman Sea is associated with fewer cut-off lows and reduced rainfall from cut-off lows. Since the thunderstorm activity is already increasing significantly in Austral spring (Allen et al., 2011), and more than half of the months in dry El Niño Cluster 2 fall in the spring season, the high percentage of weather-system-unrelated rainfall suggests the contribution of convective systems, especially in the northern and eastern subtropical parts of SEA. Along the South Coast, rainfall probably forms following the

passage of a cold front, as it is known that frontal systems bring a high percentage of rainfall in the growing season (April–October) to the South Coast of SEA (Pook et al., 2014). Most of the backward trajectories of WCB and cut-off-low rainfall come from the remote inland regions of Australia and from the Southern Ocean. These air parcels are less humid than the air parcels in wet Cluster 1, implying that trajectories from the south and remote inland are associated with less rainfall. This corroborates the findings of Brown et al. (2009) and McIntosh et al. (2012) from a climatological perspective.

In Cluster 3, the East Coast receives above-average rainfall and the area west of the Great Dividing Range below-average rainfall. In this study, we find a large region of increased blocking south of Australia centred at 120°E within a pronounced anomalous anticyclone which is associated with an increased frequency of cut-off lows at its northern flank. Moreover, the anomalous anticyclone induces anomalous easterly onshore winds, creating a situation where cut-off lows over the Tasman Sea move eastward towards Australia and bring rainfall along the East Coast to the windward side of the Great Dividing Range. This corroborates the results of Pepler et al. (2016), who find a negative correlation between zonal wind magnitude and rainfall along the East Coast of SEA from May to October. Cut-off lows contribute to the highest percentage of rainfall in wet East Coast Cluster 3. Above-average rainfall along the East Coast results particularly from an increased frequency of cut-off lows. In this context, Hendon et al. (2007) connected easterly storm track anomalies with enhanced rainfall on the southeast coast due to the combination of the increased occurrence of moist flow from the Tasman Sea and the orographic effects east of the Great Dividing Range. Backward trajectories reveal that air masses predominately originate from the Southern Ocean and move anticyclonically over the Tasman Sea towards SEA where they end up in cut-off-low rainfall in wet East Coast Cluster 3.

The rainfall anomaly pattern in wet South Coast Cluster 4 is the reversed pattern of wet East Coast Cluster 3, with below-average rainfall along the East Coast and above-average rainfall west of the Great Dividing Range. In contrast to the other clusters, we find the presence of an anomalous trough south of Australia which points to enhanced westerly winds over SEA. East of Australia, the lack of rainfall along the East Coast can be attributed to the lack of rain-bearing weather systems that are considered in this study. In connection to the "wet south" pattern, Risbey et al. (2009a) note decreased pressure and an equatorward shift of the westerly wind belt, which is in accordance with our findings. The combination of enhanced westerlies and decreased rainfall along the East Coast also agrees with the negative relationship of zonal wind magnitude

and rainfall along the East Coast found by Pepler *et al.* (2016). We find in general a low contribution of WCBs and cut-off lows to rainfall in wet South Coast Cluster 4. Rainfall along the South Coast is suggested to result primarily from fronts associated with extratropical cyclones, which corresponds to the results in the "wet south" pattern of Risbey *et al.* (2009a). Furthermore, convective systems can also contribute to rainfall primarily in the northern part of SEA during the winter–spring season. The WCB may not cover all frontal rainfall in SEA, which leads to the conclusion that non-matching rainfall further results from drizzle from shallow clouds, from occlusion fronts or from warm fronts, whose annual percentage of total rainfall exceeds 15% in SEA (Catto *et al.*, 2012a). A study by Wright (1989) also highlighted the importance of post-frontal rainfall, which is often observed in winter in southwestern Victoria and can presumably explain much of the unmatched rainfall in wet South Coast Cluster 4. Air parcels that end up in WCB rainfall show a pathway similar to dry Cluster 2 which agrees with the "dry" trajectories of Brown *et al.* (2009) and McIntosh *et al.* (2012).

## 5 | CONCLUDING REMARKS

ENSO is the primary driver of interannual rainfall variability and its positive phase – El Niño – is typically associated with below-average rainfall in SEA, especially in the winter–spring season from June to November. However, the three strong El Niño events of 1982, 1997 and 2015 showed marked differences concerning their impacts on rainfall, pointing to a nonlinear relationship between the strength of El Niño and the influence on SEA rainfall. Though previous studies mostly focus on the statistical relationship between rainfall and large-scale climate modes, the present study investigates the monthly rainfall variability in SEA during El Niño from a weather system perspective. Characteristic rainfall patterns are identified by clustering monthly rainfall anomalies in the winter–spring seasons of the last ten El Niño events. Monthly rather than seasonal averages help to explain the event-to-event variability of El Niño which has been noted in previous studies (Brown *et al.*, 2009; Taschetto and England, 2009; van Rensch *et al.*, 2019). A further benefit of this approach is that anomalous frequencies of flow features do not average out, which would be the case when averaging over an entire El Niño event.

Four different spatial rainfall anomaly patterns dominate the rainfall variability in the winter–spring season and separate wet, dry, East Coast wet and South Coast wet months in SEA. With focus on El Niño, the dry rainfall Cluster represents roughly 50% of the selected months within the period 1979–2015, which is the known average

response during El Niño. Pronounced changes of weather system frequencies occur during El Niño over SEA and vary highly with the respective monthly rainfall anomaly pattern. The most prominent changes are observed in the atmospheric blocking, WCB and cut-off-low frequencies in all clusters. There is a significant increase in the frequency of occurrence of the mentioned weather systems over SEA in the wet Cluster that is less likely to be found during El Niño events (Figure 9a). A lack of these weather systems due to blocking over the continent is observed in the dry Cluster (Figure 9b). Increased rainfall along the East Coast results from blocking south of Australia which favours the development of cut-off lows over the Tasman Sea (Figure 9c). Positive rainfall anomalies along the South Coast are associated with enhanced frontal rainfall within the equatorward-shifted storm track region (Figure 9d). The matching of rainfall with cut-off lows and WCBs shows that up to 80% of rainfall is related to two types of weather system over SEA. Convective events in the northern parts of SEA and post-frontal convective rainfall along the South Coast seem to be responsible for rainfall that cannot be attributed to WCBs and cut-off lows. That frequency changes of weather systems determine monthly rainfall anomalies is shown by decomposing rainfall anomalies into changes in frequency and intensity. The results reveal the dominance of frequency modulations in all clusters. Backward trajectories of air parcels that end up in WCB or cut-off-low rainfall in SEA highlight the pathway from the Coral Sea northeast of SEA and the striking pathway from the northwest coast of Australia for wet months (Figure 9a). A key finding is that trajectories reach SEA from the inner continent in wet months, where they continuously pick up moisture, and not (as one would intuitively expect) from the Indian or Southern Ocean. Nevertheless, pathways from the Southern Ocean and from remote inland areas of Australia are found in dry months (Figure 9b).

This study contributes towards solving the question of the strong case-to-case variability of El Niño responses in SEA. Our approach might also be suitable to shed light on the asymmetric and nonlinear response between El Niño and La Niña. Therefore, it would be intriguing to apply the utilized methods to La Niña events to also advance the dynamic understanding of the drivers leading to above-average rainfall in SEA. Although this study sheds light on the processes that drive rainfall variability during El Niño, future studies could consider further rain-bearing weather systems affecting SEA to gain a better and more complete understanding of rainfall contributors. Also, the use of a Lagrangian moisture diagnostic (Sodemann *et al.*, 2008) could provide more explicit insights into the sources of water vapour. In their study about rainfall mechanisms, van Rensch *et al.* (2019) point to the
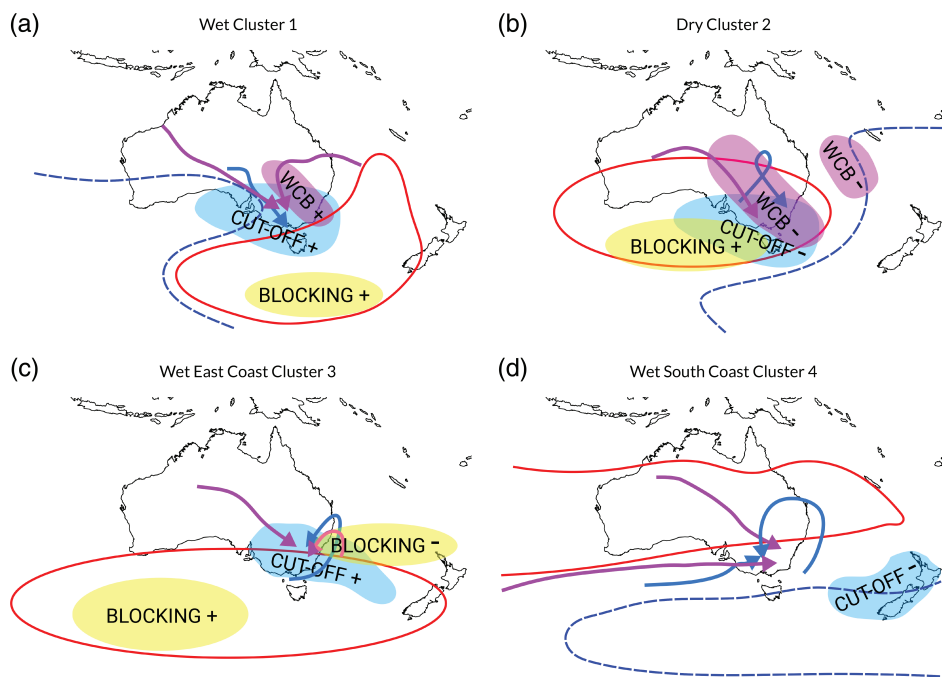
**FIGURE 9** Schematic summary of key large-scale anomalies, weather system frequency anomalies and main pathways of air parcels that end up in WCB and cut-off-low rainfall over SEA during El Niño. Red (blue) contours indicate positive (negative) geopotential anomalies at 500 hPa. With focus on the main weather systems, we display regions of significant frequency anomalies in blocking (yellow shading), cut-off lows (blue shading) and WCB ascent (pink shading) in each cluster. The signs indicate whether the frequency anomalies are positive (+) or negative (–). Coloured arrows indicate the main backward trajectory clusters of cut-off-low rainfall (blue) and WCB rainfall (pink). Only cluster-median backward trajectories are displayed which include at least 30% of all trajectories

importance of SSTs northeast of Australia as model experiments reveal that they mainly influence east Australian rainfall through changes to moisture availability. Various studies highlight the tendency for a shift of the midlatitude storm track towards higher southern latitudes due to global warming. It is thought that this shift impacts local weather and climate in SEA through a reduction of rainfall. By looking at interannual rainfall variability, our study demonstrates that it is not only the shift of the storm track that explains the rainfall anomalies, but rather the occurrence frequency of blocking and the associated development of cut-off lows in particular along the East Coast. Hence, it is of importance to further improve the understanding of blocking in the Australian region and to further assess its predictability in numerical weather prediction models on synoptic to climate time-scales.

## ORCID

*Seraphine Hauser* https://orcid.org/0000-0003-3538-270X
*Christian M. Grams* https://orcid.org/0000-0003-3466-9389
*Michael J. Reeder* https://orcid.org/0000-0002-4583-5875
*Shayne McGregor* https://orcid.org/0000-0003-3222-7042
*Andreas H. Fink* https://orcid.org/0000-0002-5840-2120
*Julian F. Quinting* https://orcid.org/0000-0002-8409-2541

## REFERENCES

Abatzoglou, J.T. (2016) Contribution of cutoff lows to precipitation across the United States. *Journal of Applied Meteorology and Climatology*, 55, 893–899.

Allan, R., Lindesay, J. and Parker, D. (1996) *El Niño Southern Oscillation and climatic variability*. CSIRO Publishing, Clayton, Victoria, Australia.

Allen, J.T., Karoly, D.J. and Mills, G.A. (2011) A severe thunderstorm climatology for Australia and associated thunderstorm environments. *Australian Meteorological and Oceanographic Journal*, 61, 143–158.

Ashcroft, L., Gergis, J. and Karoly, D.J. (2016) Long-term stationarity of El Niño–Southern Oscillation teleconnections in southeastern Australia. *Climate Dynamics*, 46, 2991–3006.

Berrisford, P., Dee, D.P., Poli, P., Brugge, R., Fielding, K., Fuentes, M., Kållberg, P., Kobayashi, S., Uppala, S.M. and Simmons, A.J. (2009). The ERA-Interim archive Version 2.0. ERA report series No. 1, ECMWF, Reading, UK.

Brown, J.N., McIntosh, P.C., Pook, M.J. and Risbey, J.S. (2009) An investigation of the links between ENSO flavors and rainfall processes in southeastern Australia. *Monthly Weather Review*, 137, 3786–3795.

Browning, K.A. (1990). Organization of clouds and precipitation in extratropical cyclones, pp. 129–153 in Extratropical Cyclones: The Erik Palmén Memorial Volume. Newton, C.W., Holopainen, E.O. (eds), American Meteorological Society, Boston, MA.

Cai, W., van Rensch, P., Cowan, T. and Sullivan, A. (2010) Asymmetry in ENSO teleconnection with regional rainfall, its multidecadal variability, and impact. *Journal of Climate*, 23, 4944–4955.

Cai, W., van Rensch, P., Cowan, T. and Hendon, H.H. (2011) Teleconnection pathways of ENSO and the IOD and the mechanisms for impacts on Australian rainfall. *Journal of Climate*, 24, 3910–3923.

Catto, J.L., Jakob, C., Berry, G. and Nicholls, N. (2012a) Relating global precipitation to atmospheric fronts. *Geophysical Research Letters*, 39(10).

Catto, J.L., Jakob, C. and Nicholls, N. (2012b) The influence of changes in synoptic regimes on north Australian wet season rainfall trends. *Journal of Geophysical Research*, 117.

Catto, J.L., Madonna, E., Joos, H., Rudeva, I. and Simmonds, I. (2015) Global relationship between fronts and warm conveyor belts and the impact on extreme precipitation. *Journal of Climate*, 28, 8411–8429.

Chung, C. and Power, S. (2017) The nonlinear impact of El Niño, La Niña and the Southern Oscillation on seasonal and regional Australian precipitation. *Journal of Southern Hemisphere Earth System Science*, 67, 25–45.

Clark, S., Reeder, M.J. and Jakob, C. (2018) Rainfall regimes over northwestern Australia. *Quarterly Journal of the Royal Meteorological Society*, 144, 458–467.

Cowan, T., van Rensch, P., Purich, A. and Cai, W. (2013) The association of tropical and extratropical climate modes to atmospheric blocking across southeastern Australia. *Journal of Climate*, 26, 7555–7569.

Dee, D.P., Uppala, S.M., Simmons, A.J., Berrisford, P., Poli, P., Kobayashi, S., Andrae, U., Balmaseda, M.A., Balsamo, G., Bauer, P., Bechtold, P., Beljaars, A.C., van de Berg, L., Bidlot, J., Bormann, N., Delsol, C., Dragani, R., Fuentes, M., Geer, A.J., Haimberger, L., Healy, S.B., Hersbach, H., Hólm, E.V., Isaksen, L., Kållberg, P., Köhler, M., Matricardi, M., Mcnally, A.P., Monge-Sanz, B.M., Morcrette, J.-J., Park, B.K., Peubey, C., de Rosnay, P., Tavolato, C., Thépaut, J.-N. and Vitart, F. (2011) The ERA-Interim reanalysis: configuration and performance of the data assimilation system. *Quarterly Journal of the Royal Meteorological Society*, 137, 553–597.

Drouard, M., Rivière, G. and Arbogast, P. (2015) The link between the North Pacific climate variability and the North Atlantic Oscillation via downstream propagation of synoptic waves. *Journal of Climate*, 28, 3957–3976.

Fogt, R.L., Bromwich, D.H. and Hines, K.M. (2011) Understanding the SAM influence on the South Pacific ENSO teleconnection. *Climate Dynamics*, 36, 1555–1576.

Hameed, S. and Yamagata, T. (2003) Possible impacts of Indian Ocean dipole mode events on global climate. *Climate Research*, 25, 151–169.

Hart, N.C.G., Gray, S.L. and Clark, P.A. (2015) Detection of coherent airstreams using cluster analysis: application to an extratropical cyclone. *Monthly Weather Review*, 143, 3518–3531.

Hartigan, J.A. and Wong, M.A. (1979) Algorithm AS 136: a k-means clustering algorithm. *Journal of the Royal Statistical Society Series C*, 28, 100–108.

Hendon, H.H., Thompson, D.W.J. and Wheeler, M.C. (2007) Australian rainfall and surface temperature variations associated with the Southern Hemisphere Annular Mode. *Journal of Climate*, 20, 2452–2467.

Jones, D., Wang, W. and Fawcett, R. (2009) High-quality spatial climate datasets for Australia. *Australian Meteorological and Oceanographic Journal*, 58, 233–248.

Kane, R.P. (1997) On the relationship of ENSO with rainfall over different parts of Australia. *Australian Meteorological Magazine*, 46, 39–49.

King, A.D., Klingaman, N.P., Alexander, L.V., Donat, M.G., Jourdain, N.C. and Maher, P. (2014) Extreme rainfall variability in Australia: patterns, drivers, and predictability. *Journal of Climate*, 27, 6035–6050.

Li, Y. and Lau, N.-C. (2012) Impact of ENSO on the atmospheric variability over the North Atlantic in late winter – role of transient eddies. *Journal of Climate*, 25, 320–342.

Madonna, E., Wernli, H., Joos, H. and Martius, O. (2014) Warm conveyor belts in the ERA-Interim dataset (1979-2010). Part I: climatology and potential vorticity evolution. *Journal of Climate*, 27, 3–26.

Marshall, G.J. (2003) Trends in the Southern Annular Mode from observations and reanalyses. *Journal of Climate*, 16, 4134–4143.

Martius, O., Schwierz, C. and Davies, H.C. (2008) Far-upstream precursors of heavy precipitation events on the Alpine south-side. *Quarterly Journal of the Royal Meteorological Society*, 134, 417–428.

McBride, J.L. and Nicholls, N. (1983) Seasonal relationships between Australian rainfall and the Southern Oscillation. *Monthly Weather Review*, 111, 1998–2004.

McIntosh, P.C., Pook, M.J., Risbey, J.S., Lisson, S.N. and Rebbeck, M. (2007) Seasonal climate forecasts for agriculture: towards better understanding and value. *Field Crops Research*, 104, 130–138.

McIntosh, P.C., Risbey, J.S., Brown, J.N. and Pook, M.J. (2012) Apparent and real sources of rainfall associated with a cutoff low in southeast Australia. *CAWCR Research Letters*, 8, 4–9. https://www.cawcr.gov.au/publications/; accessed 24 April 2020

Murphy, B.F. and Timbal, B. (2008) A review of recent climate variability and climate change in southeastern Australia. *International Journal of Climatology*, 28, 859–879.

Nicholls, N., Drosdowsky, W. and Lavery, B. (1997) Australian rainfall variability and change. *Weather*, 52, 66–72.

Nicholls, N., Lavery, B., Frederiksen, C., Drosdowsky, W. and Torok, S. (1996) Recent apparent changes in relationships between the El Niño–Southern Oscillation and Australian rainfall and temperature. *Geophysical Research Letters*, 23, 3357–3360.

Pasquier, J.T., Pfahl, S. and Grams, C.M. (2019) Modulation of atmospheric river occurrence and associated precipitation extremes in

the North Atlantic region by european weather regimes. *Geophysical Research Letters*, 46, 1014–1023.

Pepler, A., Timbal, B., Rakich, C. and Coutts-Smith, A. (2014) Indian Ocean dipole overrides ENSO's influence on cool season rainfall across the eastern seaboard of Australia. *Journal of Climate*, 27, 3816–3826.

Pepler, A.S., Alexander, L.V., Evans, J.P. and Sherwood, S.C. (2016) Zonal winds and southeast Australian rainfall in global and regional climate models. *Climate Dynamics*, 46, 123–133.

Pfahl, S., Madonna, E., Boettcher, M., Joos, H. and Wernli, H. (2014) Warm conveyor belts in the ERA-Interim dataset (1979–2010). Part II: moisture origin and relevance for precipitation. *Journal of Climate*, 27, 27–40.

Pook, M.J., McIntosh, P.C. and Meyers, G.A. (2006) The synoptic decomposition of cool-season rainfall in the southeastern Australian cropping region. *Journal of Applied Meteorology and Climatology*, 45, 1156–1170.

Pook, M.J., Risbey, J.S. and McIntosh, P.C. (2014) A comparative synoptic climatology of cool-season rainfall in major grain-growing regions of southern Australia. *Theoretical and Applied Climatology*, 117, 521–533.

Power, S., Casey, T., Folland, C.K., Colman, A. and Mehta, V. (1999) Inter-decadal modulation of the impact of ENSO on Australia. *Climate Dynamics*, 15, 319–324.

Power, S.B., Haylock, M., Colman, R. and Wang, X. (2006) The predictability of interdecadal changes in ENSO activity and ENSO teleconnections. *Journal of Climate*, 19, 4755–4771.

Reeder, M.J. and Smith, R.K. (1998). Mesoscale Meteorology, chapter 5 in Meteorology of the Southern Hemisphere. Koroly, D.J., Vincent, D.G. (eds), American Meteorological Society, Boston, MA.

Risbey, J.S., Pook, M.J., McIntosh, P.C., Ummenhofer, C.C. and Meyers, G. (2009a) Characteristics and variability of synoptic features associated with cool season rainfall in southeastern Australia. *International Journal of Climatology*, 29, 1595–1613.

Risbey, J.S., Pook, M.J., McIntosh, P.C., Wheeler, M.C. and Hendon, H.H. (2009b) On the remote drivers of rainfall variability in Australia. *Monthly Weather Review*, 137, 3233–3253.

Risbey, J.S., Mcintosh, P.C. and Pook, M.J. (2013) Synoptic components of rainfall variability and trends in southeast Australia. *International Journal of Climatology*, 33, 2459–2472.

Schemm, S., Rivière, G., Ciasto, L.M. and Li, C. (2018) Extratropical cyclogenesis changes in connection with tropospheric ENSO teleconnections to the North Atlantic: role of stationary and transient waves. *Journal of the Atmospheric Sciences*, 75, 3943–3964.

Scherrer, S.C., Croci-Maspoli, M., Schwierz, C. and Appenzeller, C. (2006) Two-dimensional indices of atmospheric blocking and their statistical relationship with winter climate patterns in the Euro-Atlantic region. *International Journal of Climatology*, 26, 233–249.

Schwierz, C., Croci-Maspoli, M. and Davies, H.C. (2004) Perspicacious indicators of atmospheric blocking. *Geophysical Research Letters*, 31

Short, A.D. (2020) *Australian Coastal Systems; beaches, barriers and sediment compartments*. Springer Nature, Cham, Switzerland.

Sodemann, H., Schwierz, C. and Wernli, H. (2008) Interannual variability of Greenland winter precipitation sources: Lagrangian moisture diagnostic and North Atlantic Oscillation influence. *Journal of Geophysical Research*, 113

Spensberger, C., Reeder, M.J., Spengler, T. and Patterson, M. (2020) The connection between the Southern Annular Mode and a feature-based perspective on Southern Hemisphere mid-latitude winter variability. *Journal of Climate*, 33, 115–129.

Sprenger, M., Fragkoulidis, G., Binder, H., Croci-Maspoli, M., Graf, P., Grams, C.M., Knippertz, P., Madonna, E., Schemm, S., Škerlak, B. and Wernli, H. (2017) Global climatologies of Eulerian and Lagrangian flow features based on ERA-Interim. *Bulletin of the American Meteorological Society*, 98, 1739–1748.

Sprenger, M. and Wernli, H. (2015) The LAGRANTO Lagrangian analysis tool – version 2.0. *Geoscientific Model Development*, 8, 2569–2586.

Tapp, R. and Barrell, S. (1984) The northwest Australian cloud band: climatology, characteristics and factors associated with development. *Journal of Climatology*, 4, 411–424.

Taschetto, A.S. and England, M.H. (2009) El Niño Modoki impacts on Australian rainfall. *Journal of Climate*, 22, 3167–3174.

Trenberth, K.E. (1991) Storm tracks in the Southern Hemisphere. *Journal of the Atmospheric Sciences*, 48, 2159–2178.

van Rensch, P., Arblaster, J., Gallant, A.J.E., Cai, W., Nicholls, N. and Durack, P.J. (2019) Mechanisms causing east Australian spring rainfall differences between three strong El Niño events. *Climate Dynamics*, 53, 3641–3659.

van Rensch, P., Gallant, A.J., Cai, W. and Nicholls, N. (2015) Evidence of local sea surface temperatures overriding the southeast Australian rainfall response to the 1997–1998 El Niño. *Geophysical Research Letters*, 42, 9449–9456.

Vera, C.S. and Osman, M. (2018) Activity of the Southern Annular Mode during 2015–2016 El Niño event and its impact on Southern Hemisphere climate anomalies. *International Journal of Climatology*, 38, 1288–1295.

Verdon, D.C. and Franks, S.W. (2005) Indian Ocean sea surface temperature variability and winter rainfall: eastern Australia. *Water Resources Research*, 41

Wernli, H. and Schwierz, C. (2006) Surface cyclones in the ERA-40 dataset (1958–2001). Part I: novel identification method and global climatology. *Journal of the Atmospheric Sciences*, 63, 2486–2507.

Wernli, H. and Sprenger, M. (2007) Identification and ERA-15 climatology of potential vorticity streamers and cutoffs near the extratropical tropopause. *Journal of the Atmospheric Sciences*, 64, 1569–1586.

Wright, W.J. (1989) A synoptic climatological classification of winter precipitation in Victoria. *Australian Meteorological Magazine*, 37, 217–229.

Wright, W.J. (1997) Tropical–extratropical cloudbands and Australian rainfall: I. Climatology. *International Journal of Climatology*, 17, 807–829